A retrograde signal from RyR1 alters DHP receptor inactivation and limits window Ca^{2+} release in muscle fibers of Y522S RyR1 knock-in mice

Zoita Andronache[a], Susan L. Hamilton[b], Robert T. Dirksen[c], and Werner Melzer[a,1]

[a]Institute of Applied Physiology, Ulm University, D-89069 Ulm, Germany; [b]Department of Molecular Physiology and Biophysics, Baylor College of Medicine, Houston, TX 77030; and [c]Department of Pharmacology and Physiology, University of Rochester Medical Center, Rochester, NY 14642

Edited by David Julius, University of California, San Francisco, CA, and approved January 16, 2009 (received for review December 15, 2008)

Malignant hyperthermia (MH) is a life-threatening hypermetabolic condition caused by dysfunctional Ca^{2+} homeostasis in skeletal muscle, which primarily originates from genetic alterations in the Ca^{2+} release channel (ryanodine receptor, RyR1) of the sarcoplasmic reticulum (SR). Owing to its physical interaction with the dihydropyridine receptor (DHPR), RyR1 is controlled by the electrical potential across the transverse tubular (TT) membrane. The DHPR exhibits both voltage-dependent activation and inactivation. Here we determined the impact of an MH mutation in RyR1 (Y522S) on these processes in adult muscle fibers isolated from heterozygous RyR1^{Y522S}-knock-in mice. The voltage dependence of DHPR-triggered Ca^{2+} release flux was left-shifted by ≈8 mV. As a consequence, the voltage window for steady-state Ca^{2+} release extended to more negative holding potentials in muscle fibers of the RyR1^{Y522S}-mice. A rise in temperature from 20° to 30 °C caused a further shift to more negative potentials of this window (by ≈20 mV). The activation of the DHPR-mediated Ca^{2+} current was minimally changed by the mutation. However, surprisingly, the voltage dependence of steady-state inactivation of DHPR-mediated calcium conductance and release were also shifted by ≈10 mV to more negative potentials, indicating a retrograde action of the RyR1 mutation on DHPR inactivation that limits window Ca^{2+} release. This effect serves as a compensatory response to the lowered voltage threshold for Ca^{2+} release caused by the Y522S mutation and represents a novel mechanism to counteract excessive Ca^{2+} leak and store depletion in MH-susceptible muscle.

dihydropyridine receptor | excitation-contraction coupling | malignant hyperthermia | mouse skeletal muscle | ryanodine receptor

Contraction and relaxation of skeletal muscle fibers involve a carefully controlled release and reuptake of Ca^{2+} ions stored in the sarcoplasmic reticulum (SR). Malignant hyperthermia (MH), a life-threatening hypermetabolic state accompanied by hyperthermia, hypoxia, hypercapnia, acidosis and muscle rigidity (1–3), results from uncontrolled release of Ca^{2+} in skeletal muscle. Episodes of MH are triggered in genetically predisposed individuals by certain pharmaceutical agents, particularly volatile anesthetics and depolarizing muscle relaxants. A large number of different mutations leading to MH susceptibility has been identified (4). These mutations primarily reside in the gene coding for the skeletal muscle isoform of the ryanodine receptor (RyR1), the major Ca^{2+} release channel of the SR.

Activation of intracellular Ca^{2+} release results from a conformational interaction between RyR1 channels in the SR and a specialized voltage-sensitive Ca^{2+} channel (L-type Ca^{2+} channel), the dihydropyridine receptor (DHPR), located in the adjacent membrane of the transverse tubular (TT) system. Upon membrane depolarization, the DHPR exhibits a fast reaction leading to Ca^{2+} release (≈10 milliseconds), a slower gating transition that activates the L-type Ca^{2+} inward current (≈100 milliseconds) and a very slow, voltage-dependent transition (seconds) that inactivates both the Ca^{2+} current and Ca^{2+} release (5). The question of whether, and if so how, MH mutations in RyR1 affect the two DHPR-controlled Ca^{2+} fluxes has been assessed in myotubes derived from primary cultured satellite cells containing either native or expressed MH mutant RyR1 channels. A consistent finding from these studies was a lowered threshold for depolarization-induced activation of Ca^{2+} release (6–9).

Recently, genetically engineered knock-in mice possessing the Y522S MH mutation have been generated (10). Mice homozygous for the mutation die during embryonic or early postnatal development. Myotubes derived from such mice exhibit left-shifted voltage-dependence of Ca^{2+} release and substantially reduced voltage- and caffeine-induced Ca^{2+} release, suggesting substantial loss of SR Ca^{2+}. A leak of Ca^{2+} from the SR was also inferred from experiments using transient co-expression of mutant (Y522S) and wild-type RyR1 in RyR1-deficient (dyspedic) myotubes to mimic the heterozygous state (9). Heterozygous Y522S mice live and breed normally, but are susceptible to fulminant MH-like events after a heat challenge or exposure to volatile anesthetics. Myotubes from these mice, however, showed no evidence of uncompensated SR Ca^{2+} depletion (10).

The goals of the present study were to assess the functional consequences of the Y522S MH mutation in RyR1 to excitation–contraction coupling in adult muscle of heterozygous mice and to identify possible mechanisms that limit leakage of Ca^{2+} from the SR. For this purpose, we used enzymatically isolated short muscle fibers and measured L-type Ca^{2+} currents, gating charge movements and intracellular Ca^{2+} release under voltage clamp conditions. We determined in parallel the voltage dependence of activation and inactivation of both Ca^{2+} current and Ca^{2+} release in this preparation, and we provide evidence for a modulatory alteration in DHPR inactivation that counteracts the enhanced sensitivity of the release mechanism to activation by voltage associated with the Y522S mutation.

Results

Voltage-Dependent Activation of Ca^{2+} Release and Ca^{2+} Current. Using a two-electrode voltage clamp system, we recorded the L-type Ca^{2+} inward current and derived the SR Ca^{2+} release flux from simultaneous measurements of voltage-activated fura-2 fluorescence signals as described by Ursu et al. (11).

Fig. 1 shows representative experiments on single *interosseus* muscle fibers. An initial voltage pulse to + 20 mV was followed by a series of pulses covering the voltage range between −60 and + 50 mV (Fig. 1*A*). Measured fluorescence ratios, calculated Ca^{2+} release flux traces, and Ca^{2+} inward currents are presented

Author contributions: Z.A., R.T.D., and W.M. designed research; Z.A. performed research; S.L.H. contributed new reagents/analytic tools; Z.A. and W.M. analyzed data; and Z.A., S.L.H., R.T.D., and W.M. wrote the paper.

The authors declare no conflict of interest.

This article is a PNAS Direct Submission.

[1]To whom correspondence should be addressed at: Ulm University, Institute of Applied Physiology, Albert-Einstein-Allee 11, D-89069 Ulm, Germany. E-mail: werner.melzer@uni-ulm.de.

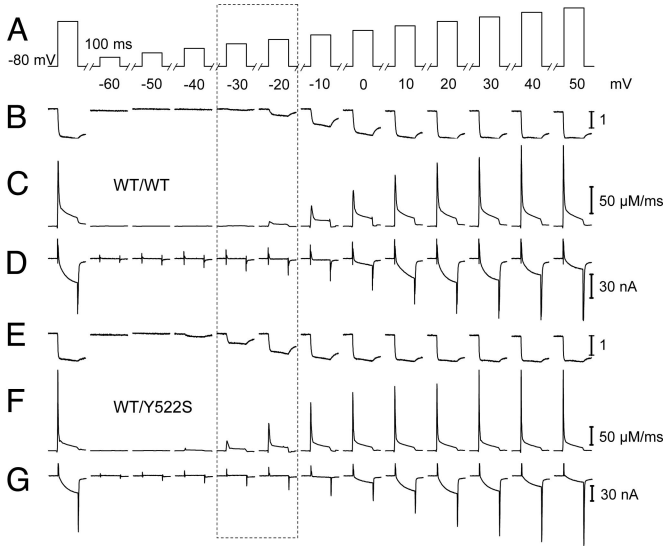

Fig. 1. Voltage-dependent activation of Ca^{2+} release flux and Ca^{2+} entry. Depolarizing voltage steps (100 milliseconds) with progressively increasing amplitude were applied from a holding potential of −80 mV (*A*). The time interval between pulses was 60 seconds. Fura-2 fluorescence ratios (*B* and *E*) were used to calculate Ca^{2+} release flux (*C* and *F*). Simultaneously recorded Ca^{2+} inward currents (*D* and *G*). Representative traces of a WT/WT (*B–D*) and a WT/Y522S fiber (*E–G*), respectively.

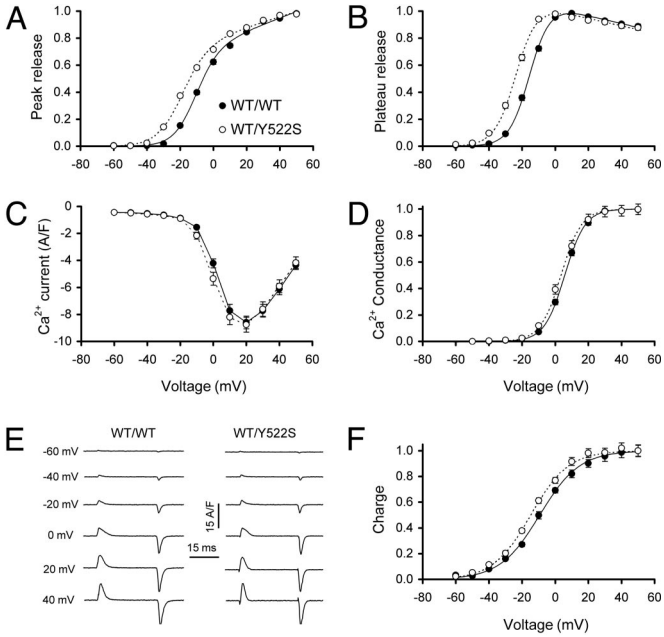

Fig. 2. Voltage dependence of Ca^{2+} release flux and Ca^{2+} inward current. Voltage dependence of the peak (*A*) and plateau (*B*) components of Ca^{2+} release flux normalized to the maximal values. Plateau values were determined by averaging release flux values between 25 and 75 milliseconds during the pulse. (*C*) Voltage dependence of Ca^{2+} inward current density. (*D*) Normalized Ca^{2+} conductance derived from *C*. (*E*) Representative traces of intramembrane charge movements obtained with 30 milliseconds pulses. (*F*) Normalized charge–voltage relationships determined by integrating the nonlinear current at the onset of each pulse. Parameter values obtained by optimization in the removal fit analysis were as follows (for a detailed description and definitions, see (11)): WT/WT: $k_{off,Dye}$ = 35.6 ± 2.9 s^{-1}, $k_{on,S}$ = 17.8 ± 1.6 μM^{-1} s^{-1}, $k_{off,S}$ = 5.7 ± 0.7 s^{-1}, k_{uptake} = 5.4 × 10^3 ± 0.7 × 10^3 s^{-1}. WT/Y522S: $k_{off,Dye}$ = 45.6 ± 4 s^{-1} (P = 0.05), $k_{on,S}$ = 21.3 ± 3.4 μM^{-1} s^{-1} (P = 0.37), $k_{off,S}$ = 9.5 ± 0.9 s^{-1} (P = 0.001), k_{uptake} = 8.1 × 10^3 ± 1.2 × 10^3 s^{-1} (P = 0.06). The voltage dependence of release flux was fitted by the function $F(V) = (a + bV)/(1 + exp((V_{1/2}–V)/k))$. The parameters $V_{1/2}$, k, a and b had the following mean values: Peak (WT/WT): −11.5 ± 0.7 mV, 6.9 ± 0.2 mV, 0.0047 ± 0.0005 and 0.76 ± 0.02. Peak (WT/Y522S): −19.7 ± 0.7 mV (P = 3.6 × 10^{-11}), 7.7 ± 0.2 mV (P = 0.01), 0.0038 ± 0.0004 (P = 0.13) and 0.80 ± 0.016 (P = 0.08). Plateau (WT/WT): −15.2 ± 0.6 mV, 6.1 ± 0.1 mV, −0.0029 ± 0.0004 and 1.03 ± 0.007. Plateau (WT/Y522S): −23.6 ± 0.7 mV (P = 8.1 × 10^{-12}), 6.4 ± 0.2 mV (P = 0.28), −0.0028 ± 0.0004 (P = 0.79) and 1.0 ± 0.006 (P = 0.02). Absolute values of peak release at + 50 mV were 150 ± 16.6 and 164 ± 17.6 μM/ms in WT/WT and WT/Y522S, respectively (P = 0.59), assuming 40% loading of the fibers (see Materials and Methods). The voltage dependence of the leak-corrected Ca^{2+} current density was fitted by the function $I(V) = g_{Ca,max}(V - V_{Ca})/(1 + exp((V_{1/2}–V)/k))$. The parameters $g_{Ca,max}$, V_{Ca}, $V_{1/2}$ and k had the following mean values: WT/WT: 174 ± 11.9 S F^{-1}, 74.1 ± 2.4 mV, 5.7 ± 0.6 mV and 6.2 ± 0.3 mV, respectively. WT/Y522S: 183.1 ± 8.5 S F^{-1} (P = 0.56), 71.6 ± 2.3 mV (P = 0.47), 3.4 ± 1 mV (P = 0.04) and 6.2 ± 0.2 mV (P = 0.9), respectively. Mean linear capacitance was 6.5 ± 0.4 nF and 5.6 ± 0.3 nF (P = 0.1), respectively. Boltzmann fit parameters q_{max}, $V_{1/2}$ and k of charge–voltage relationships were 28.5 ± 1.2 nC μF^{-1}, −9.4 ± 1.2 mV and 12 ± 0.6 mV for WT/WT and 25.2 ± 0.9 nC μF^{-1} (P = 0.036), −14.8 ± 1.3 mV (P = 0.015) and 11.4 ± 0.4 mV (P = 0.42) for WT/Y522S, respectively. Mean linear capacitance in these experiments was 3.7 ± 0.3 nF and 3.3 ± 0.1 nF (P = 0.27), respectively. P values in brackets indicate results of the t test. The number of experiments for Ca^{2+} release flux, Ca^{2+} current and charge movement were and 30, 29, and 9 for WT/WT and 23, 22 and 9 for WT/Y522S, respectively.

in Figs. 1*B*, 1*C*, and 1*D* for a WT/WT fiber and in Figs. 1*E*, 1*F*, and 1*G* for a WT/Y522S fiber, respectively. The most striking effect observed in the mutants was a hyperpolarizing shift in the voltage threshold for activation of Ca^{2+} release (Fig. 1, dotted frame).

Fig. 2*A–D* compares the average voltage dependence of Ca^{2+} release flux and Ca^{2+} entry from 30 WT/WT fibers (filled circles) and 23 WT/Y522S fibers (open circles) obtained from experiments such as those shown in Fig. 1. Figures 2*A* and 2*B* compare the voltage dependence of peak and plateau release flux (for definition, see legend), whereas Figs. 2*C* and 2*D* compare the Ca^{2+} current– and conductance–voltage relationships. Clearly, Ca^{2+} release activation in WT/Y522S fibers is shifted to more negative potentials. The difference in the voltages of half-maximal activation ($V_{1/2}$) of release was −8.2 mV, whereas the change in $V_{1/2}$ of Ca^{2+} conductance activation was only −2.3 mV. These results in muscle fibers are consistent with previous findings in myotubes (9, 10), indicating that the Y522S MH mutation preferentially lowers the voltage threshold for activation of Ca^{2+} release.

Figure 2*E* shows recordings of intra-membrane charge movements (gating currents) obtained with 30-millisecond test depolarizations to the indicated voltages after blocking the Ca^{2+} current. These non-linear capacitive currents are thought to reflect the voltage-dependent conformational changes of the DHPR that control Ca^{2+} release. The voltage dependence of charge movement activation (Fig. 2*F*) was also displaced to more negative potentials in WT/Y522S fibers compared to WT/WT fibers, but less than that observed for peak Ca^{2+} release (−5.4 mV vs. −8.2 mV).

Voltage-Activated Ca^{2+} Release Permeability. After the initial large peak, Ca^{2+} release flux rapidly falls until it reaches a slowly declining plateau (Fig. 3*A*). There is evidence that the slow decline in the plateau phase results from gradual depletion of the SR of its stored Ca^{2+} (12). Assuming a constant residual release flux during the plateau component, the total flux trace can be corrected for the putative depletion (dotted trace in Fig. 3*A*) as shown by Gonzalez and Rios (13). The analysis leads to an estimate of the initial SR Ca^{2+} content (before the pulse) using a least-squares optimization procedure. Figure 3*B* shows the putative Ca^{2+} content of the SR derived in this way (initial) and the content remaining at the end of each activating voltage pulse (final). The voltage dependence of the latter in WT/Y522S fibers

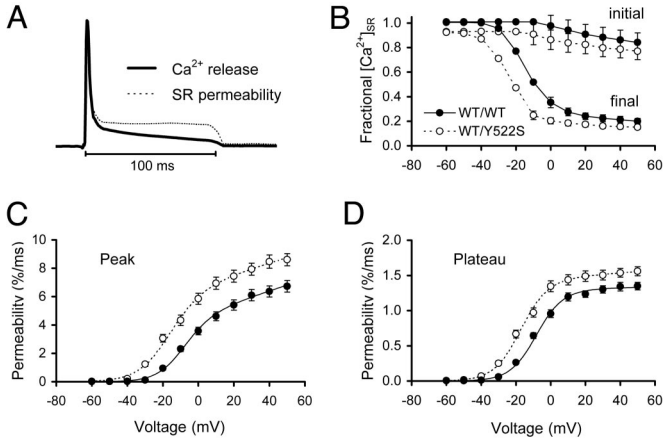

Fig. 3. Voltage-activated SR Ca^{2+} permeability and SR Ca^{2+} content. (*A*) Ca^{2+} release flux (continuous trace) and depletion-corrected flux (SR permeability, dotted trace). (*B*) SR Ca^{2+} content at the beginning (initial) and at the end (final) of the depolarizing pulse for different test voltages. For large voltages (from 0 mV to + 50 mV in WT/WT and −10 mV to + 50 mV in WT/Y522S) the initial SR content was obtained by analyzing the corresponding Ca^{2+} release flux traces. For smaller pulses this parameter was set to the mean value of the estimates obtained between −10 and + 10 mV and at the leading test pulse at +20 mV. The mean initial SR content (total releasable Ca^{2+} referenced to myoplasmic water volume) estimated for + 50 mV is not significantly higher in WT/WT fibers (2.17 ± 0.2 mM, $n = 30$) compared to WT/Y522S fibers (1.98 ± 0.2 mM, $n = 23$, $P = 0.53$). Note that these concentration estimates assume 40% loading of fibers with EGTA from the current passing pipette (see Materials and Methods). (*C* and *D*) Voltage-dependence of peak (*C*) and plateau (*D*) permeabilities derived from the data in Fig. 2.

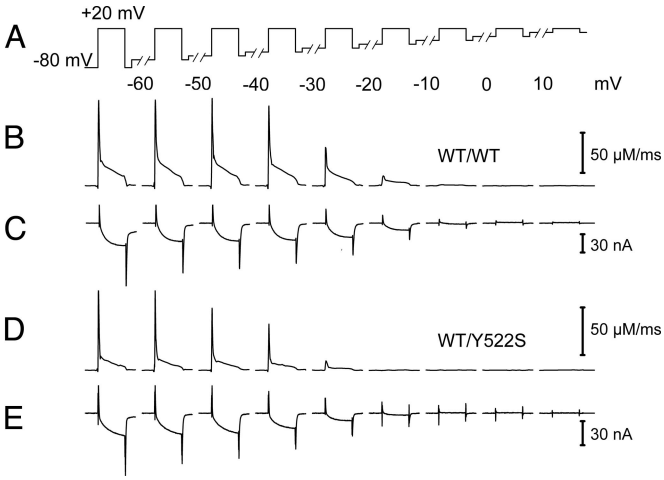

Fig. 4. Voltage-dependent inactivation of Ca^{2+} release and Ca^{2+} inward current. (*A*) Progressively more depolarized conditioning potentials were applied to inactivate DHPR voltage sensors. Each conditioning depolarization lasted 30 seconds and was followed by a 100-millisecond test pulse to +20 mV. (*B–E*) Representative traces of simultaneously recorded Ca^{2+} release fluxes (*B* and *D*) and Ca^{2+} inward currents (*C* and *E*) in WT/WT (*B* and *C*) and WT/Y522S fibers (*D* and *E*).

is shifted to more negative voltages, similar to those observed for the Ca^{2+} release activation curve. The results indicate that during the course of a 100-millisecond pulse to +50 mV, the Ca^{2+} load of the SR drops to 19.1% and 15.5% of its initial content in WT/WT and WT/Y522S fibers, respectively. The estimate of the mean initial load was slightly smaller in the WT/Y522S fibers, but this difference was not statistically significant ($P = 0.51$, +50 mV).

Depletion-corrected fluxes are proportional to the voltage-activated permeability of the SR for Ca^{2+}. Mean peak and plateau permeability plotted against voltage are shown in Figs. 3*C* and 3*D*, respectively. The maximal values (at + 50 mV, in %/ms) were 8.6 ± 0.4 vs. 6.7 ± 0.4 (peak) and 1.56 ± 0.07 vs. 1.35 ± 0.05 (plateau) for WT/Y522S vs. WT/WT, respectively. These differences were statistically significant ($P = 0.0029$ and $P = 0.015$, respectively). Both peak and plateau permeabilities were shifted to more negative potentials (by 7.9 mV and 9.1 mV, respectively) in WT/Y522S fibers.

Voltage-Dependent Inactivation. RyR1-mediated Ca^{2+} release triggered by the voltage sensor is also subject to a slow voltage-dependent inactivation process that is a characteristic of the DHPR. This phenomenon was first studied as a spontaneous relaxation in single frog muscle fibers exposed to depolarizing solutions (14). Within several seconds, it leads to almost complete abolition of the voltage-activated Ca^{2+} fluxes (i.e., both entry and release).

To determine the degree of inactivation at different voltages, we applied the voltage clamp protocol shown in Fig. 4*A*. Starting from a −80 mV holding potential, the membrane potential was progressively depolarized. After a 30-second time interval at the respective membrane potential, a 100-millisecond test pulse to +20 mV was applied to determine the fraction of Ca^{2+} release and L-type Ca^{2+} conductance that remained available for activation. Figure 4 shows that both Ca^{2+} release (Figs. 4*B* and 4*D*) and Ca^{2+} current (Figs. 4*C* and 4*E*) evoked by the test pulse are progressively reduced with increasing conditioning depolarization. Surprisingly, Ca^{2+} release and influx were more susceptible to inactivation by predepolarization in the WT/Y522S fibers (Figs. 4*D* and 4*E*) than in the WT/WT fibers (Figs. 4*B* and 4*C*). This observation is confirmed by comparing the mean availability curves that display fractional activation (at + 20 mV) vs. conditioning voltage (Fig. 5). For both Ca^{2+} release (Fig. 5*A*) and Ca^{2+} current (Fig. 5*B*), the curves of the WT/Y522S fibers are substantially shifted to more negative potentials (≈10 mV). Specifically, the values for the voltage of half-maximal inactivation ($V_{1/2}$) were −44.8 and −34.4 mV for Ca^{2+} release (A) and −32.1 and −22.8 mV for Ca^{2+} current (B) in WT/Y522S and WT/WT fibers, respectively.

Window Ca^{2+} Fluxes. Figures 6*A* and 6*B* combine the activation and inactivation curves obtained in the preceding experiments. For the voltage dependence of Ca^{2+} release activation, we chose the normalized voltage dependence of plateau permeability. The

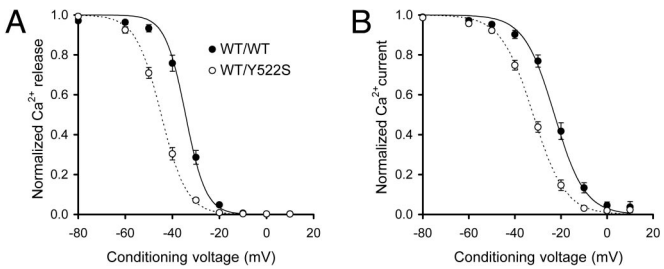

Fig. 5. Voltage dependence of inactivation of Ca^{2+} release and Ca^{2+} conductance. Fractional availability of peak Ca^{2+} release flux (*A*) and Ca^{2+} current (*B*) plotted as a function of conditioning voltage. In WT/Y522S fibers, both inactivation curves are shifted to more hyperpolarized potentials compared with WT/WT fibers. The voltage dependence of each relationship was fitted with a conventional Boltzmann function (continuous and dotted lines). The parameters $V_{1/2}$ and k had the following values: Release: WT/WT; −34.4 ± 0.9 mV and 4.3 ± 0.3 mV ($n = 17$); WT/Y522S: −44.8 ± 0.8 mV ($P = 6.7 \times 10^{-10}$) and 5.4 ± 0.2 mV ($P = 0.002$) ($n = 19$). Current: WT/WT; −22.8 ± 1.2 mV and 6.6 ± 0.5 mV ($n = 17$); WT/Y522S: −32.1 ± 0.9 mV ($P = 5 \times 10^{-7}$) and 6.9 ± 0.2 mV ($P = 0.55$) ($n = 18$).

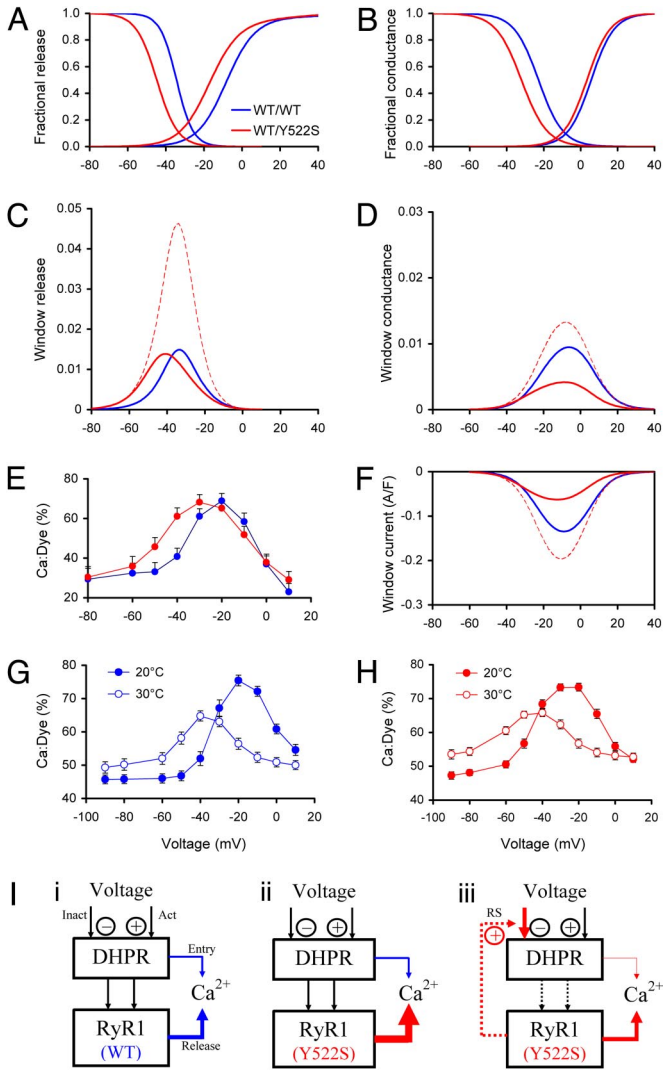

Fig. 6. Alterations of window Ca^{2+} fluxes in WT/Y522S fibers. (*A*) Normalized voltage dependence of release activation (plateau permeability) and inactivation curves replotted from the data shown in Fig. 3*D* and Fig. 5*A*. (*B*) Normalized voltage dependence of Ca^{2+} channel conductance activation and inactivation curves replotted from the data shown in Fig. 2*D* and Fig. 5*B*. (*C*) Voltage dependence of window Ca^{2+} release (fraction of maximum) calculated from the product of the corresponding normalized activation and inactivation curves shown in (*A*) (continuous blue and red lines). (*D*) Voltage dependence of fractional window Ca^{2+} conductance calculated from the product of the corresponding activation and inactivation curves shown in (*B*). (*E*) Steady-state Ca^{2+} increase (expressed as fraction of dye bound to Ca^{2+}) at the end of each conditioning voltage during the inactivation protocol (Fig. 4). (*F*) Voltage dependence of window L-type current derived from (*D*). The red dashed curves in (*C*), (*D*), and (*F*) were calculated under the assumption of no change in the voltage dependence of inactivation. (*G* and *H*) Effect of temperature on window Ca^{2+} elevation. The numbers of experiments were 17 (WT/WT) and 37 (WT/Y522S), respectively. (*I*) Model to summarize alterations in Ca^{2+} release control caused by the Y522S mutation in RyR1.

overlap between the Ca^{2+} release activation and inactivation curves in Fig. 6*A* predicts a "window of voltages" around the union of the two curves in which some activation of Ca^{2+} release will occur while inactivation is not yet complete, thus generating a steady-state flux of Ca^{2+} from the SR. A corresponding window conductance is predicted by the overlapping regions of the curves shown in Fig. 6*B*.

Figures 6*C* and 6*D* show "window release" and "window conductance" constructed as the product of the WT/WT (solid blue lines) and WT/Y522S (solid red lines) activation and inactivation curves. The analysis reveals a similar maximal value for the steady-state window release in WT/WT and WT/Y522S fibers. However, an ≈8-mV hyperpolarizing shift of the window maximum is observed in WT/Y522S fibers. On the other hand, the peak of L-type Ca^{2+} channel window conductance is reduced and minimally shifted in WT/Y522S fibers. Figure 6*F* shows the voltage dependence of the "window current" calculated by multiplying the traces in Fig. 6*D* with $g_{max}(V - V_{Ca})$ derived from the fit of the current–voltage relationship (Fig. 2*C*). The red dashed curves in Figs. 6*C*, 6*D*, and 6*F* show window release and window conductance (current), calculated under the assumption that the voltage dependence of inactivation was not shifted. The maximal window fluxes, in particular, release, would be substantially larger in WT/Y522S fibers in the absence of the observed hyperpolarizing shift in the voltage dependence of inactivation.

Results in Fig. 6*C* indicate that the maximum window release would be three-fold larger in WT/Y522S fibers if the shift of the activation curve of release were the only effect of the mutation. That this is not the case could be independently derived from the fura-2 fluorescence recordings in the experiments assessing the voltage dependence of inactivation. Fura-2 fluorescence ratiometry allowed us to determine steady-state myoplasmic Ca^{2+} levels at the end of each long conditioning depolarization. The measured values display a bell-shaped voltage dependence (Fig. 6*E*), as would be expected to result from the presence of a window release. Furthermore, a hyperpolarizing shift (by 10 mV) of the maximum was observed in WT/Y522S fibers, whereas the maximal values were similar in WT/WT and WT/Y522S fibers, consistent with the calculations shown in Fig. 6*C* (solid lines).

For simplicity, we assumed that the plateau permeability remains constant and that its voltage dependence determined from 100-millisecond pulses is representative of the steady state. Possible deviations from these assumptions (15) may explain why the absolute voltages do not perfectly coincide in the two ways of defining the Ca^{2+} release window in Figs. 6*C* and 6*E*. Nevertheless, both determinations show very similar differences between WT/Y522S and WT/WT fibers, i.e., a left shift and a broadening of the window.

Because heat challenge triggers MH in WT/Y522S mice, we also investigated the impact of raising ambient temperature on window Ca^{2+} elevation. To minimally disturb the intracellular conditions in these experiments, we voltage-clamped the fibers using two sharp microelectrodes after loading them with membrane permeant fura-2-AM. An increase in bath temperature from 20° to 30 °C was applied. As shown in Fig. 6*G* and 6*H*, the change in temperature caused a similar change in amplitude and hyperpolarizing shift (≈20 mV) in the window Ca^{2+} elevation in both WT/WT and WT/Y522S fibers.

Together, these results demonstrate that window Ca^{2+} flux occurs at more negative potentials in WT/Y522S muscle fibers. This effect is increased at a higher ambient temperature, and the size of the window flux is effectively limited by a displacement in the voltage-dependence of steady-state inactivation.

Discussion

Alterations in Voltage-Dependent Activation and Window Ca^{2+} Release. Myotubes derived from homozygous Y522S knock-in mice exhibit a marked reduction in depolarization- and drug-induced Ca^{2+} release (10), consistent with a lower SR Ca^{2+} content due to leakage as found in experiments using transient expression of mutant RyR1 in HEK293 cells (16) and dyspedic myotubes (9). Experiments on myotubes derived from heterozygous WT/Y522S mice, on the other hand, showed no evidence for uncompensated SR Ca^{2+} leak (10). In agreement with these findings, our data indicate that total SR Ca^{2+} content is essen-

tially unaltered in fibers of adult WT/Y522S mice and that maximal depolarization-induced Ca^{2+} release flux is not significantly different between WT/WT and WT/Y522S fibers. The slight reduction in Ca^{2+} store content seen in our permeability analysis (Fig. 3*B*) may indicate a certain degree of increased SR Ca^{2+} leak that is almost completely compensated for by Ca^{2+} reuptake. Differences in the degree of SR Ca^{2+} leak between experiments conducted in myocytes from knock-in mice and transient overexpression in HEK293 cells or dyspedic myotubes most likely reflect compensatory mechanisms commandeered in the mice to limit SR Ca^{2+} loss (see below).

The activation curve for Ca^{2+} release permeability in WT/Y522S fibers was shifted by ≈8 mV to more negative potentials compared with WT/WT, whereas the voltage dependence of L-type Ca^{2+} current activation was almost unchanged. This observation is qualitatively similar to results reported by Dietze et al. (8) for primary cultured porcine myotubes exhibiting homozygous expression of the R615C mutation. A selective left shift of the activation curve for Ca^{2+} release was also found by Avila and Dirksen (9) using various mutant RyR1s expressed in dyspedic myotubes and by Chelu et al. (10) using myotubes of homozygous and heterozygous $RyR1^{Y522S}$ knock-in mice.

By applying a simple model suggested by Dietze et al. (8), our data from mutant fibers could be well fitted with a single 2.2-fold increase in the closed-to-open equilibrium constant of the RyR1. The same model also predicts a left shift in the charge–voltage relationship. A comprehensive quantitative explanation of the consequences of MH mutations on DHPR-triggered SR Ca^{2+} release will require considerably more complex models (17) that take into account the clustered arrangement of the RyR1 (18) and local Ca^{2+}-dependent positive and negative regulatory mechanisms.

Interestingly, raising ambient temperature by 10 °C caused a strong effect on the voltage window for steady-state Ca^{2+} release (Fig. 6*G* and 6*H*). The scale of the signals may be influenced by the temperature dependence of various factors including Ca^{2+} pump rate and properties of intrinsic buffers and the indicator dye (19). However, the strong hyperpolarizing shift reflects temperature-dependent changes in channel gating consistent with that reported recently (20). This effect places the window close to the normal resting potential in the mutant fibers. Increased fiber fragility prevented similar measurements of window Ca^{2+} release at temperatures higher than 30 °C. However, extrapolation of the observed changes to higher temperatures could contribute to the heat-induced MH phenotype of WT/Y522S mice (10, 20). Our findings also suggest a critical role of the resting membrane potential for maintaining proper Ca^{2+} homeostasis in WT/Y522S muscle, as only a small depolarization in the resting potential would produce a continuous flux of Ca^{2+} from the SR. Indeed, sustained graded membrane depolarization can occur, for example, after strenuous exercise as a consequence of microlesions or activity-induced accumulation of potassium in the TT lumen and may therefore contribute to the stress sensitivity of these mice.

Altered Voltage-Dependent Inactivation. A surprising result of the present study is the observation that the voltage-dependence of DHPR inactivation is shifted to more negative potentials in muscle fibers of WT/Y522S knock-in mice. In the absence of this shift, the steady-state window of Ca^{2+} release in WT/Y522S fibers (Fig. 6*C*, red dashed line) would exhibit a considerably larger amplitude, thus permitting a substantially greater degree of steady-state SR Ca^{2+} leak. However, our results demonstrate that the effect of enhanced activation on window flux amplitude is dramatically attenuated by the displacement of the steady-state Ca^{2+} release availability curve to more negative potentials. Consequently steady-state Ca^{2+} leak in the window region is significantly decreased (Fig. 6*C* and 6*E*, continuous red traces). Moreover, steady-state Ca^{2+} entry caused by the L-type Ca^{2+} channel window conductance, which is small compared with release (11), is even further reduced (Fig. 6*D* and 6*F*, continuous red traces).

The fact that the shift in the inactivation involves both Ca^{2+} release and Ca^{2+} entry indicates that the Y522S mutation in RyR1 influences the inactivation gating properties of the DHPR. The proposed mechanism is depicted in Fig. 6*I*. Under normal conditions (*i*), window Ca^{2+} release and window Ca^{2+} entry result from a delicate balance between DHPR activation (Act) and inactivation (Inact). In the absence of any compensatory mechanisms (*ii*), the MH mutation in RyR1 would increase window Ca^{2+} release as a result of a selective hyperpolarizing shift in the voltage dependence of Ca^{2+} release. However, a parallel hyperpolarizing shift in the voltage dependence of DHPR inactivation caused by a retrograde signal (RS) from RyR1 (*iii*) prevents an increase in steady-state window release and entry. One form of RyR1-DHPR retrograde signaling has been discovered in myotubes of RyR1-null mice (dyspedic mice), which exhibit substantially smaller L-type currents than normal myotubes (21–24). This likely results from the loss of physical contact between the two proteins. Multiple regions of the RyR1 are candidates for direct interaction with the DHPR (25). However, the feedback proposed here may also take an indirect route. For instance, local elevations in Ca^{2+} concentration resulting from the mutant RyR1 might activate Ca^{2+}-dependent enzymes that lead to modification of the DHPR complex either by proteolysis (e.g., calpain) or by the production of reactive oxygen or nitrogen species (20). Potential targets for such modifications are the α_{1S} polypeptide and its ancillary subunits. Notably, the γ_1 subunit exhibits a pronounced effect on DHPR inactivation (26). Finally, a long-term change in the expression of proteins that modify or modulate the DHPR may also be involved. The precise mechanism by which the Y522S mutation in RyR1 alters the voltage dependence of DHPR inactivation will require further investigation.

In conclusion, our results indicate that the increase in uncompensated SR Ca^{2+} leak observed at rest following transient overexpression of the Y522S RyR1 mutant in myotubes (9) is effectively suppressed after long-term expression of a normal compliment of wild-type and mutant RyR1s in adult muscle fibers of WT/Y522S mice. The ability of the mutation to augment the tendency of RyR1 to open is, however, still reflected in a left shift in both the voltage dependence for Ca^{2+} release activation and window release. We also find that an increase in ambient temperature further shifts the voltage dependence of window calcium flux to more negative voltages, an effect that contributes to the heat stress intolerance of WT/Y522S knock-in mice. The finding of altered voltage dependence of steady-state DHPR inactivation is indicative of a novel type of retrograde RyR1-DHPR coupling that promotes the inactivation process. This effect results in a compensatory protective mechanism that limits excessive SR Ca^{2+} release and store depletion, in particular under conditions of partial depolarization.

Materials and Methods

Preparation. Male WT/WT (mean age, 28 weeks; range, 19–50 weeks) and WT/Y522S (mean age, 29 weeks; range, 20–45 weeks) littermates in the C57/Bl6 genetic background (10) were used for the experiments. Mice were killed by exposure to CO_2 followed by cervical dislocation. All animal procedures were approved by the local animal care committee. Interosseus muscle fiber dissociation was performed as previously described (11).

Experimental Solutions. External bath solution (in mM): 130 TEA-OH, 130 HCH_3SO_3, 2 $MgCl_2$, 10 $CaCl_2$, 5 4-aminopyridine (4-AP), 10 HEPES, 0.001 TTX, 5 glucose, 0.05 *N*-benzyl-*p*-toluene sulfonamide (BTS), pH 7.4. Perfusion pipette solution (in mM): 145 CsOH, 110 aspartic acid, 0.75 Na_2ATP, MgATP (5.16 Mg^{2+}, 4.25 ATP), 1.5 $CaCl_2$, 10 HEPES, 15 EGTA, 0.2 fura-2, 5 $Na_2CreatinePO_4$, pH 7.2.

Voltage Clamping and Data Analysis. The experimental design was as described (11, 27). Briefly, isolated fibers were voltage-clamped with a two-electrode system (Axoclamp 2B, Axon Instruments) and imaged using a fluorescence microscope (Axiovert 135 TV, 40x/0.75W objective, Zeiss). Fibers were dialyzed with the fura-2– containing solution in the current-passing electrode. Unless otherwise stated, experimental temperature was 20–22 °C and the holding potential −80 mV. Ca^{2+} signals and L-type Ca^{2+} currents were simultaneously recorded at 2 kHz. To construct Ca^{2+} current–voltage relationships, we averaged the last 10 milliseconds of each depolarization step. Ratiometric Ca^{2+} transients were subjected to a removal model fit analysis as originally described by Melzer et al. (28) to calculate the flux of Ca^{2+} from the SR (11, 29). The pipette concentrations of EGTA and fura-2 were used as the buffer concentrations for the removal analysis. Because the estimates of Ca^{2+} release flux amplitude (and of SR Ca^{2+} content) are proportional to the actual intracellular EGTA concentration, these values were scaled down by a factor of 0.4 to account for the mean fractional loading of the fiber at the time of recording determined in other experiments (11). SR Ca^{2+} permeability was calculated according to Gonzalez and Rios (13). To record non-linear charge movements, the data sampling rate was changed to 10 kHz. Ca^{2+} currents were blocked by adding 0.5 mM $CdCl_2$ and 0.3 mM $LaCl_3$ to the external bath solution. Correction for linear capacitive currents was performed by analog compensation and subsequent off-line subtraction of appropriately scaled control pulse responses (−20 mV from the holding potential). Small residual leak currents were compensated by subtracting sloping lines fitted to intervals of 14 and 54 milliseconds that started 13 milliseconds after the onset and end of the pulse, respectively. The voltage dependence of activation and inactivation curves was described by Boltzmann functions, except for the activation of Ca^{2+} release and permeability, in which a linear term was included to account for a deviation at large depolarizations (11).

Statistics. Averaged data are presented and plotted as means ± SEM (n = number of experiments). Student's two-tailed t test for two independent populations was used to test for statistical significance ($P < 0.05$).

ACKNOWLEDGMENTS. We gratefully acknowledge the support by F. Lehmann-Horn, the director of the Institute of Applied Physiology. We thank R.P. Schuhmeier and D. Ursu for developing analysis software, M. Orynbayev for designing a heating device, and K. Fuchs, A. Riecker, and E. Schoch for expert technical help. This research was supported by grants from the Deutsche Forschungsgemeinschaft (ME-713/18–1 and ME-713/19–1 to W.M.) and the National Institutes for Health (AR44657 to R.T.D. and AR53349 and AR050503 to S.L.H.). Z.A.'s position was partially funded by research-training grant HPRN-CT-2002–00331 from the European Commission (to W.M.).

1. MacLennan DH, Phillips MS (1992) Malignant hyperthermia. *Science* 256:789–794.
2. Lehmann-Horn F, Jurkat-Rott K (1999) Voltage-gated ion channels and hereditary disease. *Physiol Rev* 79:1317–1372.
3. Rosenberg H, Davis M, James D, Pollock N, Stowell K (2007) Malignant hyperthermia. *Orphanet J Rare Dis* 2:21.
4. Robinson R, Carpenter D, Shaw MA, Halsall J, Hopkins P (2006) Mutations in RYR1 in malignant hyperthermia and central core disease. *Hum Mutat* 27:977–989.
5. Melzer W, Herrmann-Frank A, Lüttgau HC (1995) The role of Ca^{2+} ions in excitation-contraction coupling of skeletal muscle fibres. *Biochim Biophys Acta* 1241:59–116.
6. Gallant EM, Jordan RC (1996) Porcine malignant hyperthermia: Genotype and contractile threshold of immature muscles. *Muscle Nerve* 19:68–73.
7. Gallant EM, Balog EM, Beam KG (1996) Slow calcium current is not reduced in malignant hyperthermic porcine myotubes. *Muscle Nerve* 19:450–455.
8. Dietze B, Henke J, Eichinger HM, Lehmann-Horn F, Melzer W (2000) Malignant hyperthermia mutation Arg615Cys in the porcine ryanodine receptor alters voltage dependence of Ca^{2+} release. *J Physiol* 526:507–514.
9. Avila G, Dirksen RT (2001) Functional effects of central core disease mutations in the cytoplasmic region of the skeletal muscle ryanodine receptor. *J Gen Physiol* 118:277–290.
10. Chelu MG et al. (2006) Heat- and anesthesia-induced malignant hyperthermia in an RyR1 knock-in mouse. *FASEB J* 20:329–330.
11. Ursu D, Schuhmeier RP, Melzer W (2005) Voltage-controlled Ca^{2+} release and entry flux in isolated adult muscle fibres of the mouse. *J Physiol* 562:347–365.
12. Schneider MF, Simon BJ, Szücs G (1987) Depletion of calcium from the sarcoplasmic reticulum during calcium release in frog skeletal muscle. *J Physiol* 392:167–192.
13. Gonzalez A, Ríos E (1993) Perchlorate enhances transmission in skeletal muscle excitation-contraction coupling. *J Gen Physiol* 102:373–421.
14. Hodgkin AL, Horowicz P (1960) Potassium contractures in single muscle fibres. *J Physiol* 153:386–403.
15. Royer L, Pouvreau S, Rios E (2008) Evolution and modulation of intracellular calcium release during long-lasting, depleting depolarization in mouse muscle. *J Physiol* 586:4609–4629.
16. Tong J, McCarthy TV, MacLennan DH (1999) Measurement of resting cytosolic Ca^{2+} concentrations and Ca^{2+} store size in HEK-293 cells transfected with malignant hyperthermia or central core disease mutant Ca^{2+} release channels. *J Biol Chem* 274:693–702.
17. Stern MD, Pizarro G, Ríos E (1997) Local control model of excitation-contraction coupling in skeletal muscle. *J Gen Physiol* 110:415–440.
18. Block BA, Imagawa T, Campbell KP, Franzini-Armstrong C (1988) Structural evidence for direct interaction between the molecular components of the transverse tubule/sarcoplasmic reticulum junction in skeletal muscle. *J Cell Biol* 107:2587–2600.
19. Larsson D, Larsson B, Lundgren T, Sundell K (1999) The effect of pH and temperature on the dissociation constant for fura-2 and their effects on [Ca(2+)] (*i*) in enterocytes from a poikilothermic animal, Atlantic cod (Gadus morhua). *Anal Biochem* 273:60–65.
20. Durham WJ et al. (2008) RyR1 S-nitrosylation underlies environmental heat stroke and sudden death in Y522S RyR1 knockin mice. *Cell* 133:53–65.
21. Nakai J et al. (1996) Enhanced dihydropyridine receptor channel activity in the presence of ryanodine receptor. *Nature* 380:72–75.
22. Grabner M, Dirksen RT, Suda N, Beam KG (1999) The II-III loop of the skeletal muscle dihydropyridine receptor is responsible for the bi-directional coupling with the ryanodine receptor. *J Biol Chem* 274:21913–21919.
23. Avila G, Dirksen RT (2000) Functional impact of the ryanodine receptor on the skeletal muscle L-type Ca^{2+} channel. *J Gen Physiol* 115:467–480.
24. Dirksen RT (2002) Bi-directional coupling between dihydropyridine receptors and ryanodine receptors. *Front Biosci* 7:d659–d670.
25. Sheridan DC et al. (2006) Bidirectional signaling between calcium channels of skeletal muscle requires multiple direct and indirect interactions. *Proc Natl Acad Sci USA* 103:19760–19765.
26. Andronache Z et al. (2007) The auxiliary subunit gamma 1 of the skeletal muscle L-type Ca^{2+} channel is an endogenous Ca^{2+} antagonist. *Proc Natl Acad Sci USA* 104:17885–17890.
27. Ursu D, Schuhmeier RP, Freichel M, Flockerzi V, Melzer W (2004) Altered inactivation of Ca^{2+} current and Ca^{2+} release in mouse muscle fibers deficient in the DHP receptor gamma1 subunit. *J Gen Physiol* 124:605–618.
28. Melzer W, Ríos E, Schneider MF (1986) The removal of myoplasmic free calcium following calcium release in frog skeletal muscle. *J Physiol* 372:261–292.
29. Schuhmeier RP, Melzer W (2004) Voltage-dependent Ca^{2+} fluxes in skeletal myotubes determined using a removal model analysis. *J Gen Physiol* 123:33–51.